

Permeability of open-pore microcellular materials

Jean-François Despois, Andreas Mortensen *

Laboratory for Mechanical Metallurgy, Department of Materials, Ecole Polytechnique Fédérale de Lausanne (EPFL), Room MX-D 140, Station 12, CH-1015 Lausanne, Switzerland

Received 26 August 2004; received in revised form 22 November 2004; accepted 23 November 2004
Available online 24 December 2004

Abstract

A simple microstructure-based model is proposed for the permeability of open-pore microcellular materials. The permeability of aluminium open-pore foams produced using the replication process is measured using water or glycerine as the fluid, varying the average cell size (75 and 400 μm) and the relative density from 12% to 32%. Data show the expected dependence on the square of the pore size and agree with other experimental data in the literature for coarser aluminium foams produced by a casting process. The analysis agrees well with present and published experimental data over the entire density range. The model also agrees with the predictions of Du Plessis et al. for low-density foams.

© 2004 Acta Materialia Inc. Published by Elsevier Ltd. All rights reserved.

Keywords: Infiltration; Aluminium; Foams; Porous material; Permeability

1. Introduction

When pores of a metal foam are interconnected, a fluid such as air or water can be made to flow through the material. Heat can then be exchanged between the fluid and the solid foam, or alternatively the foam can be used to change the fluid, acting as a filter, mixer, electrode or catalyser. Open-cell metal foams can thus provide performance advantages in forced convection heat-exchangers for electronics or aerospace applications [1–9], in the flow-field of bipolar/end plates of stacked polymer electrolyte fuel cells [10], in aerospace fluid storage tanks, and as battery electrodes [11,12].

In many such applications, the resistance to fluid flow through the porous material is an important parameter. The lower this resistance is, the less energy is spent pushing the fluid through the foam; however, high resistance to flow can also bring benefits, such as a desirable transition in reactant mass transport mode in fuel cells [10],

or an increased effectiveness of heat transfer between fluid and solid in compact heat-exchangers [5,6].

Flow resistance of an incompressible Newtonian fluid through a porous medium is generally measured by the excess pressure ΔP that must be applied on the fluid to cause it to flow at steady state with a given unidirectional average velocity through a unit length of the porous medium. For velocity and pore size ranges generally encountered in engineering, the law governing such unidirectional fluid flow is the Dupuit–Forchheimer modification of Darcy's law:

$$-\frac{\partial P}{\partial x} = \frac{\mu}{K} v_0 + \rho C v_0^2, \quad (1)$$

where P is pressure in the fluid and x is distance along the direction of macroscopic fluid flow, μ is the dynamic viscosity of the fluid and ρ its density. The Darcian permeability K and the form coefficient C are characteristics of the porous medium. Velocity v_0 is the “superficial” (or “Darcian” or “seepage”) fluid velocity, defined as the number of cubic metres of fluid seeping in one second through one square meter of porous medium cut perpendicularly to the average direction of fluid flow.

* Corresponding author. Tel.: +41 21 693 2912; fax: +41 21 693 4664.

E-mail address: andreas.mortensen@epfl.ch (A. Mortensen).

Eq. (1) implies a transition from viscosity-dominated flow at low velocities to inertia-dominated flow at higher velocities. For a given porous medium, the transition takes place around a certain value of the fluid Reynold's number Re , defined on the basis of a characteristic dimension δ of the porous medium (δ is often taken as \sqrt{K} or otherwise is the diameter of pores or solid elements making the porous medium). This transition Re value is often taken to be near 0.1; however, in practice it depends strongly on the choice made in defining δ and on the nature of the porous medium, varying significantly as these parameters vary (by roughly three orders of magnitude [13]). At yet higher values of Re , roughly one hundred to one thousand times above that which characterizes the first transition away from purely viscous flow, turbulence sets in. This causes C to become velocity-dependent in a transition region (an effect at times expressed by a cubic term) and then to settle at a different value for very high flow rates. Underlying fundamentals can be found in [13–16].

At low fluid velocities, Eq. (1) simplifies to Darcy's law:

$$v_0 = -\frac{K}{\mu} \frac{\partial P}{\partial x} \quad (2)$$

and flow is entirely governed by viscous friction within the fluid. Assuming a non-deforming solid, governing equations are the Stokes and continuity equations in the fluid, with an imposed average flow velocity and the condition that, everywhere along the fluid/porous medium interface, the fluid velocity be zero. The permeability K is thus the basic linear property characterizing porous media with regard to fluid flow; it is analogous in that sense to elastic constants with regard to deformation [17]. Elementary dimensional analysis dictates that K always be proportional to the square of any characteristic dimension δ of the porous medium, such as its average pore or particle size.

The permeability of open-pore cellular materials has been the subject of several prior investigations. Metal foams have often been studied in such investigations, either because they are far more convenient to use than polymer foams (polymer foams are weak, so they often deform as they are traversed by a flowing fluid, e.g. [18–21]), or because of their potential in specific engineering applications mentioned above. Characteristic foam parameters K and C of Eq. (1) have thus been measured by various authors for nickel foams [22,23] or for ERG's cast aluminium foams, at times compressed beforehand by plastic deformation along one direction to improve their heat-transfer characteristics (this, of course, renders the foams anisotropic) [3,5,6,9,16,24–27].

Several approaches have been used to predict the permeability of open-pore foams. Tube-bundle theories (e.g. [28–30]) are one option; however, these lack a solid theoretical foundation and require a “structural” or

“geometrical” (i.e., a fitting) parameter, which reduces their utility. One can assimilate the open-pore microcellular material to an assemblage of fibres, on the reasoning that an open-pore metal foam is mostly composed of straight elongated rods resembling randomly oriented fibers; this approach was followed by Lu et al. [4].

An approach specifically conceived for open-pore cellular materials was proposed by Du Plessis et al. [31–33]. Their model uses the volumetric averaging approach to calculate the resistance to flow of a Newtonian fluid through a periodic unit cell shaped as a cube containing three perpendicular solid rods of rectangular cross-section situated along three of its edges. The model shows good predictive power when confronted with experimental data on open-cell ERG aluminium foams of high porosity; however, the porosity range explored is rather narrow, i.e., between 92% and 96%. Also, pre-calibration of the model against experimental data was needed to fix the ratio between the edge length of the assumed cubic unit cell and the average foam pore diameter; in other words, the model contained an adjustable parameter [32]. Fourie and Du Plessis et al. [24] later resolved the issue by calculating the ratio between their cubic cell size and that of a more realistic tetrakaidecahedral foam unit cell having the same specific surface. The resulting expression showed good agreement with cited data; however, these data were for flow at velocities above the Darcian regime.

Bhattacharya et al. [26] also adapted the model of Du Plessis et al. with a different estimation of the unit cell size, additionally modifying the evaluation of the tortuosity parameter to account for the finite size of nodes in the foam. These authors also found good agreement with their own experimental data. More recently, Boomsma et al. [34] have simulated flow through a tetrakaidecahedral unit cell representative of open-pore foams, the precise shape of which was calculated to respect capillary equilibrium (and was hence very realistic). Their predictions were compared with data for a slightly more dense foam of identical pore size in the Darcian flow regime. Agreement between calculated and measured pressure drops (and hence between permeabilities) was within 25%, which is very good since permeability data generally vary over wide ranges. Poor agreement between experiment and theory was on the other hand found in a recent study of flow through open-pore ceramic foams, motivating the authors to propose a semi-empirical correlation involving fitting parameters [35].

We present in what follows a somewhat different approach towards modelling the permeability of open-pore cellular materials. The analysis is both simple and realistic, and is applicable also to foams of high volume fractions solid. We then present experimental data for the permeability of aluminium foams produced by the replication process. We finally confront the model with these data and also with data from the literature.

2. Theory

There exist several approaches to estimate the permeability of porous media; one is to identify, when possible, “bottlenecks” along the flow path of the fluid, and assimilate the total resistance to flow of the porous medium to that encountered at the bottlenecks only. This is reasonable in estimating permeability, because the linear dependence of flow resistance on the square of the fluid passage diameter ensures that bottlenecks, if they exist, mostly govern the overall rate of flow (as we all know from pouring liquid out of a bottle). As an example of the approach, a “lubrication theory” approximation of flow past the narrowest constriction between parallel fibres works quite well in estimating the permeability of fibre bundles in cross-flow at high solid volume fraction [36–39].

Many open-pore cellular materials contain nearly spherical pores connected with one another through more or less circular “windows”, each delineated by solid struts that narrow to a thin edge along the perimeter of the window. Two types of open-pore cellular material fall in this category, Fig. 1. Open-pore polymeric (e.g. polyurethane) foams produced from closed-cell froths by bursting the thin cell walls are one, Fig. 1(a). Metal or ceramic foams produced by casting into a mold shaped by using such polymeric foams as a fugitive pattern obviously fall in the same category. Also, foams produced by coating such polymeric foams with a thicker layer (several μm) of metal or ceramic (e.g. [40,41]) have a closely related structure. A second type of foam falling into this category is that of replicated foams. These are produced by infiltrating the open space left between bonded leachable particles with a liquid that is later solidified [42–44]; Fig. 1(b) provides an example.

In open-cell foams such as these, there are obvious “bottlenecks”, namely the windows that connect one pore to the next. Representing these as circular holes of uniform size cut through a thin solid plane, we can use the expression given by Happel and Brenner [45] for the pressure drop ΔP experienced by a fluid of viscosity μ traversing, at volumetric rate Q (m^3/s) and in creeping flow, a circular aperture of radius c :

$$\Delta P = \frac{3Q\mu}{c^3}. \quad (3)$$

The orientation of these circular windows is random in the foam; as a consequence the local rate of flow of the fluid through the windows varies from near-zero for windows oriented along the average flow direction, to a value well above the average fluid velocity for windows oriented perpendicular to the macroscopic direction of fluid flow. There are at least seven windows per pore, the number being nearer 14 in low-density foams [46]: clearly each pore has, on each side, one window that is close to being perpendicular to the average direc-

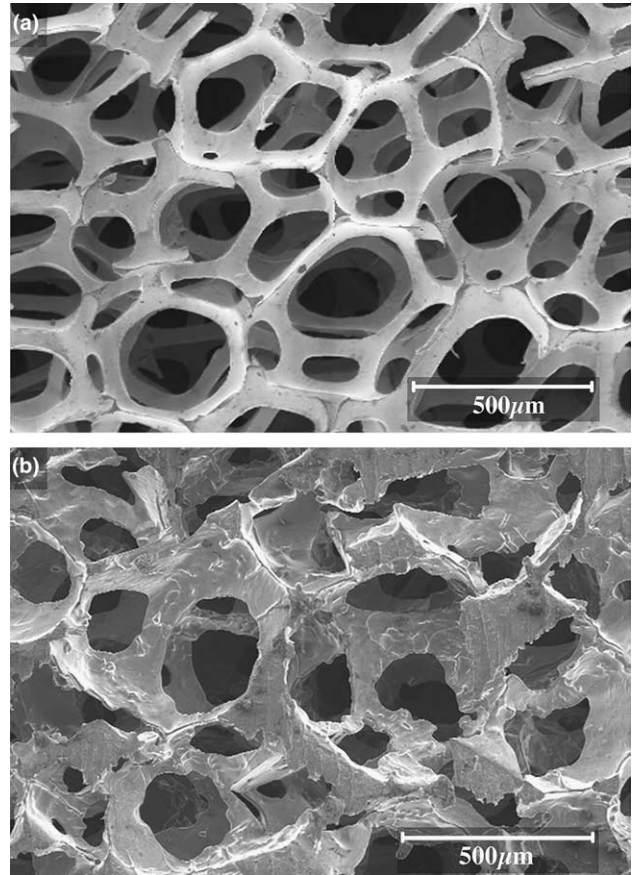


Fig. 1. Examples of open-pore cellular materials containing nearly spherical pores connected with one another through windows. (a) Polyurethane foam, made conductive by coating with a very thin ($0.1 \mu\text{m}$) layer of nickel by cathodic magnetron sputtering (at Nitech, Corp., France, sample courtesy of Dr. Michel Croset, France) and (b) pure aluminium foam produced by replication at EPFL [44]. Both open-cell foams show characteristic struts, nodes and windows connecting and restricting fluid flow between open cells.

tion of fluid flow (this is quite apparent when observing the structures of Fig. 1). We therefore assume that, of all windows lining a pore, there is one on either side that is far better oriented than all others with regard to the average direction of fluid flow: essentially all fluid passing through the pore thus enters through a single inlet window on one side and exits through a single outlet window on the opposite side of the pore. If there are n pores in a given volume of foam, each window belonging to two pores, there then is an equal number n of “active” windows, i.e., of windows that are crossed by a significant flux of flowing fluid.

The size of the windows can be calculated by drawing a parallel between the shape of pores in these foams and that of sintered or pressed equisized (initially) spherical particles in a dry powder compact. The microstructure is essentially the same, except that solid and pore are inverted in space. We can then use relationships that have been derived for the latter situation, giving the average

window area (equal to the average contact area at necks between two particles), a [47] as

$$a = \frac{\pi}{3} \left(\frac{\Delta - \Delta_0}{1 - \Delta_0} \right) r^2, \quad (4)$$

where Δ is the solid density in a particle compact (the pore volume fraction in a foam), Δ_0 is the initial packing density of the spherical particles ($\Delta_0 = 0.64$ for random dense packing of monosized spheres) and r is the initial particle radius (close to the average pore radius in a foam).

The average window radius c in the foam is thus

$$c = \left(\frac{a}{\pi} \right)^{1/2} = \frac{1}{\sqrt{3}} \left(\frac{\Delta - \Delta_0}{1 - \Delta_0} \right)^{1/2} r. \quad (5)$$

Consider now a thin square slab of open-pore microcellular foam material, of thickness $2r$ and of 1 m side lengths. The number of (whole) pores contained in this slab, n , is given by

$$n = \frac{3\Delta}{2\pi r^2}. \quad (6)$$

Essentially all fluid flowing through this thin slab of foam traverses one and only one window (since the slab is $2r$ thick). With the assumptions made above, the total number of windows being traversed by fluid in this thin slab of material is also n . If Q is the volumetric rate of fluid flowing through each active window, the superficial velocity v_0 is then

$$v_0 = nQ = \frac{3\Delta}{2\pi r^2} Q. \quad (7)$$

Since across this slab the average pressure difference ΔP is simply $2r$ times the macroscopic pressure gradient ($-\partial P/\partial x$), insertion of Eqs. (3) and (5) into Eq. (7) yields

$$v_0 = -\frac{\Delta r^2}{\pi\mu} \left[\frac{\Delta - \Delta_0}{3(1 - \Delta_0)} \right]^{3/2} \frac{\partial P}{\partial x}. \quad (8)$$

By comparison with Darcy's law, Eq. (2), the permeability K is

$$K = \frac{\Delta r^2}{\pi} \left[\frac{\Delta - \Delta_0}{3(1 - \Delta_0)} \right]^{3/2}. \quad (9)$$

We have used the simplified expression for a given in [47]. The derivation is repeated in Appendix A using the full expression derived by Arzt [46], to show that the simplification in expression (4) makes an insignificant difference in the final result (Eq. (9)).

3. Experimental procedures

Pure sodium chloride was sieved to obtain particles of controlled size and then cold isostatically pressed at various pressures to produce porous preforms from 67% to 86% dense. Two average salt particle sizes were used, namely $75\ \mu\text{m}$ (CPI salt, >98% NaCl with 1–2 pct. $\text{Ca}(\text{PO}_4)_2$ anticaking agent, purchased from Salines de Bex, Bex, Switzerland) and $400\ \mu\text{m}$ (Fluka 71382, >99.5% NaCl, from Fluka Chemie GmbH, Buchs, Switzerland). The particle size distribution for each of these two batches of sieved powder was measured with a laser diffraction analyser (*Mastersizer* from Malvern, Worces-

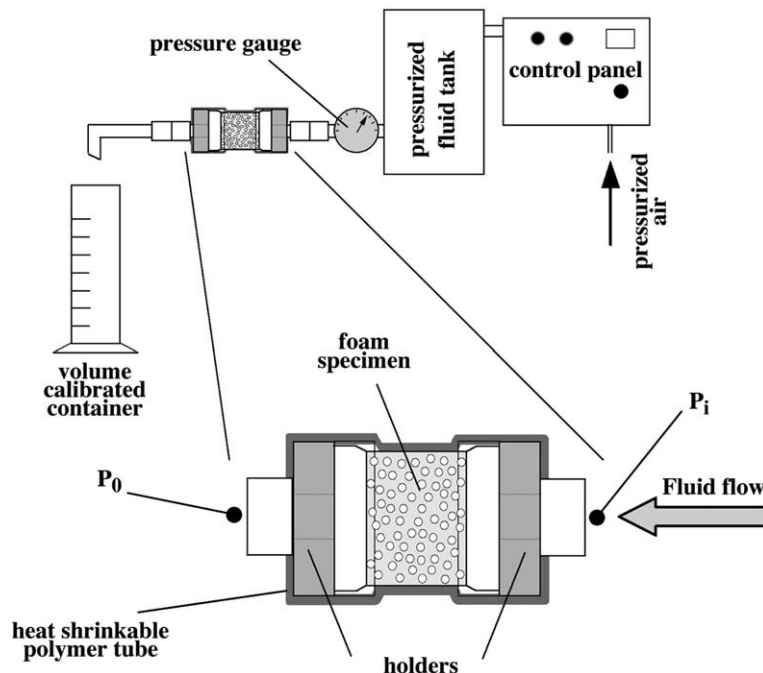


Fig. 2. Schematic of the permeability measurement apparatus, detailing the set-up used to hold and seal the foam specimen during forced fluid flow.

tershire, UK). This technique derives particle diameters from measured equivalent projected sphere areas for each particle characterized. Resulting particle diameter distributions featured an average value of 74 μm and a standard deviation of 22 μm for the finer powder, and an average diameter of 383 μm with a standard deviation of 190 μm for the coarser powder. In what follows the designations “75” and “400 μm ” are used to designate these two salt particle types and by implication the average size of pores in each of the resulting foams. In the calculations, however, the measured average diameter values given above were used.

Preforms were infiltrated at 710 $^{\circ}\text{C}$ with molten aluminium (99.99% pure, from VAW, Grevenbroich, Germany) under argon gas pressurized to 80 bars for the 75 μm particles and 2 bars for the 400 μm particle preforms. The resulting Al–NaCl composites were then machined into cylinders 20 mm in length and 25 mm in diameter. The salt was subsequently removed by dissolution in distilled water, leaving cylindrical samples of open-cell pure aluminium foam.

The permeability was measured by flowing liquid at steady state through the foams using the set-up sketched in Fig. 2. The liquid was distilled water for the specimen with pores 75 μm in diameter and a solution of 85% of glycerine in 15% water for the specimens with 400 μm pores. The fluid pressure at the entry of the specimen, P_i , was set at a fixed value up to 5 bars. The pressure at the outlet was simply the atmospheric pressure P_0 ; it was measured before each experiment. To ensure that no fluid flows along the outer side-surface of the specimens, the foam cylinders were sealed into a heat-shrinkable polymer tube designed to fit perfectly to the specimen shape and squeeze it along its sides when contracting. For given pressures the fluid volumetric flow rate R was determined by measuring the time to fill a container of precisely known volume. To check for constancy of the flow rate, 5–10 successive measurements of the flow rate were performed for each experiment.

Darcy’s original law [48] modified to account for the properties of the porous medium and the fluid [49,50] can then be written in the following form [13,14]:

$$\frac{R}{A} = q = \frac{K}{\mu} \left(\frac{P_i - P_0}{L} \right), \quad (10)$$

where R is the volumetric flow rate (m^3/s); A the cross-section of the specimen (m^2); q the apparent flow velocity (equal to the superficial velocity v_0) (m/s); K the permeability (m^2); μ the viscosity of the fluid (Pa s); and L is the length of the specimen (m).

The viscosity of the water–glycerine solution was measured as a function of temperature using a parallel plate rheometre (*ARES* from Rheometric Scientific, TA instruments, Alzenau, Germany) and was found to be $\mu = 157 \times 10^{-3}$ (Pa s) at 20 $^{\circ}\text{C}$. The viscosity of water is taken to be equal to 1.002×10^{-3} (Pa s) at 20 $^{\circ}\text{C}$ [51].

4. Results

Plots of the measured flow rate versus applied pressure gradient are given in Fig. 3. These plots are linear, showing that flow is indeed in the regime of validity of Darcy’s law. Multiplying the slope of these lines with the viscosity μ of the fluid yields the permeability K . Resulting values for K are given in Table 1. These values, normalized by the pore size squared d^2 , are plotted as a function of the foam volume fraction solid V_s (or relative density, equal to $1 - \Delta$), Fig. 4. One sees that K decreases rapidly above $V_s = 0.30$, corresponding to Δ values approaching $\Delta_0 = 0.64$. Additional data points

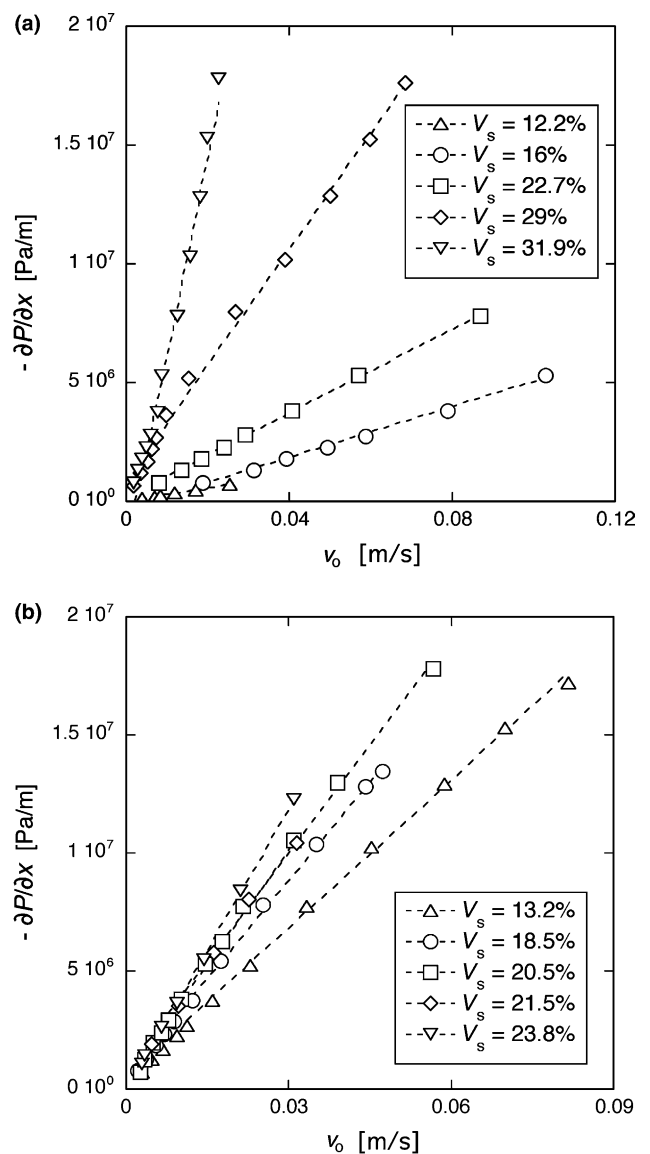


Fig. 3. Pressure gradient ($-\partial P/\partial x$), measured on foams of different density V_s plotted as a function of the superficial fluid velocity v_0 . (a) shows the results for 75 and (b) 400 μm pore foams. Note that according to Eq. (1) the slope of the dotted lines (regression straight lines) corresponds to K/μ .

Table 1

Measured values of permeability K for replicated aluminium foams as a function of the pore size d and the foam relative density V_s

Pore size $d = 75 \mu\text{m}$		Pore size $d = 400 \mu\text{m}$	
V_s (-)	K (m^2)	V_s (-)	K (m^2)
0.122	$3.56\text{E} - 11$	0.132	$7.64\text{E} - 10$
0.160	$1.88\text{E} - 11$	0.185	$5.74\text{E} - 10$
0.227	$1.12\text{E} - 11$	0.205	$5.22\text{E} - 10$
0.290	$4.07\text{E} - 12$	0.215	$4.91\text{E} - 10$
0.319	$1.23\text{E} - 12$	0.238	$4.04\text{E} - 10$

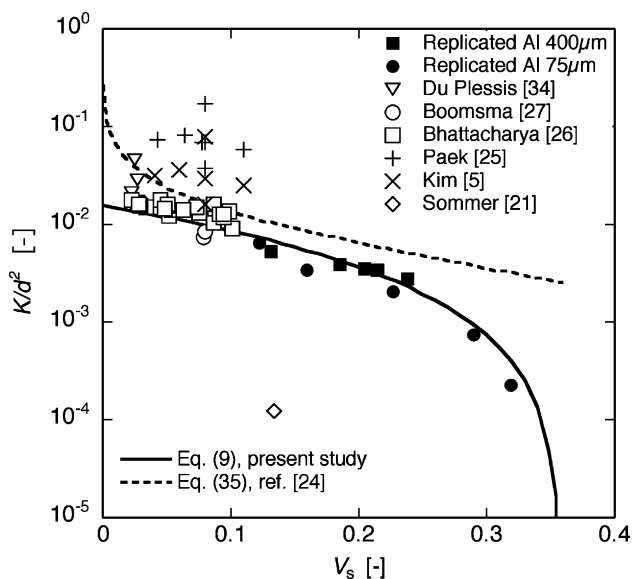


Fig. 4. Evolution of the permeability K normalized by the pore size squared d^2 as a function of the foam density V_s . Discrete points are the measured data from the present study (the two symbols correspond to the two different pore size classes that are investigated, i.e., 75 and 400 μm) and data from publications in the literature [5,21,25–27,32]. The lines are predictions according to Eq. (9) from the present study and Eq. (35) from [24].

from the literature for cast open-pore aluminium foams [5,21,25–27,32] are added to the plot after division of reported permeabilities by reported average pore diameters squared.

5. Discussion

Defining a Reynold's number for flow in these experiments as

$$Re = \frac{\rho\sqrt{K}}{\mu}q, \quad (11)$$

where ρ is the density of the fluid, one finds that Re is under 0.5 for all specimens tested here. It is, hence, not surprising that flow remain in the Darcian regime for all present experimental data.

Measured values for the permeability adimensionalized by dividing measured values for K by the average salt particle (and hence pore) diameter squared, d^2 , collapse onto a single curve, Fig. 4, as expected from dimensional analysis. Also, with the exception of data by Kim, Paek et al., permeability data from the present study and the literature are consistent with one another, within experimental scatter.

Predictions of Eq. (9) are also plotted in Fig. 4. Agreement with experiment is found to be very satisfying, especially in view of the simplicity of the final expression obtained. That the model overpredicts somewhat the permeability of the foams is not unexpected: as seen in Fig. 1(b), the present aluminium foams are more irregular in their structure than is assumed in a model that supposes all “windows” to be circular and regular, and all pore surfaces to be smooth.

Predictions from another expression for the permeability of microcellular materials are also plotted in Fig. 4, namely the model of Du Plessis et al. [31–33] as improved by Fourie and Du Plessis, Eq. (35) in [24]. As seen, in the range $5\% = V_s = 20\%$, Eq. (9) and the expressions derived by Du Plessis et al. agree very well.

At higher densities, i.e., for $V_s > 20\%$, Eq. (9) exhibits a gradual decrease in permeability, a feature that is indeed shown by the experimental data but not predicted by Du Plessis's model. The reason is that, contrary to that model, the present derivation predicts that, as V_s approaches 36%, the average inter-pore window shrinks and closes off. This conforms with reality, since pores in a foam become isolated spherical bubbles above 64% porosity.

Finally, an isolated diamond-shaped data point is seen in the lower-half of Fig. 4. This is the permeability deduced by extrapolation to zero strain of measurements reported in [21] for the permeability to flowing ethylene glycol of hydrostatically compressed polyurethane foams. As seen, this experimental point lies far below values for other foams and predictions. The reason for this discrepancy is clear on examination of the microstructure of the foam, Fig. 3 of [21]: although the foam structure is overall that assumed here, namely of spherical voids connected by roughly circular windows, the windows are very small. These windows are small perforations in otherwise intact bubble membranes of the closed-cell foam precursor to this open-pore foam. This points to the importance of respecting, in the application of Eq. (9), the premise of its derivation, namely that *all* membrane material in the closed-cell froth from which the open-pore foam may be produced be broken (the slight anisotropy along the rise direction in polymer foams is, comparatively, of minor importance).

As the foam density tends to zero the present model fails, since predicted permeabilities remain finite. This

is an obvious consequence of the assumption made in the derivation: no matter how low the density of the foam, the assumed windows remain and constrain flow – this, of course, cannot be. Eq. (9) is therefore only to be used for solid foams containing at least a few percent solid by volume. This is in contrast with Eq. (35) of [24], which behave properly as V_s approaches zero. We note in passing that replicated foams containing only a few percent solid are unrealistic: pores in the leachable powder preform close off and therefore cannot be infiltrated when they represent only a few percent of volume [49].

6. Conclusion

- A simple “bottleneck” model of the Darcian permeability K of open-pore microcellular materials made of fully interconnected near-spherical pores is used to derive a simple expression for K as a function of foam density and pore diameter (Eq. (9) above).
- Fluid permeability tests have been conducted on replicated open-cell aluminium foams with porosities comprised between 60% and 90% and with two different pore sizes, i.e., 75 and 400 μm . Experimental data normalized by the pore diameter squared collapse onto a single curve and agree with other data reported in the literature for metal foams of higher pore volume fraction.
- The derived expression for K presented in Eq. (9) agrees well with experimental data for the permeability of microcellular open-pore metal foams.

Acknowledgements

This work was funded by the Swiss National Science Foundation, Project No. 200020-100179/1. The authors thank the Laboratory of Polymer and Composite Technology of EPFL for lending the permeability measurement equipment, Miss. Barbara Rast who adapted this equipment for testing of aluminium foam specimens and who made preliminary measurements, Mr. Y. Conde and Mr. M.E. Jan who helped with the measurements, and Dr. Michel Croset, formerly of Nitech Corp., France, for sending to us the material that is photographed in Fig. 1(a).

Appendix A

Eq. (9) predicts the permeability of a porous material as a function of its porosity and pore size. This equation can be written as a function of the average surface area,

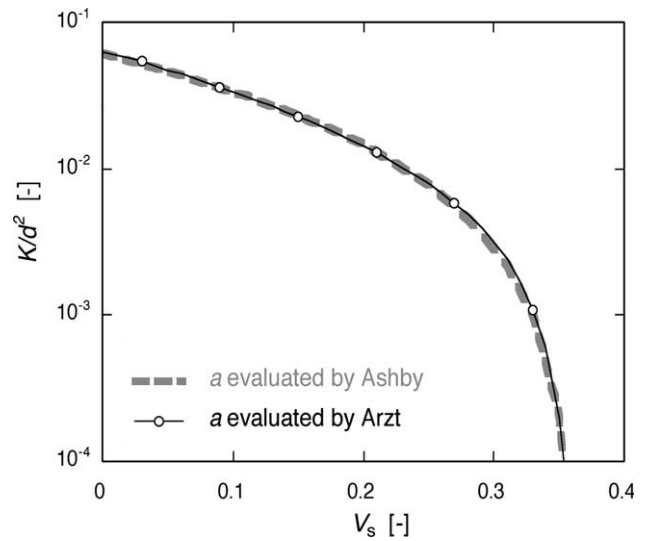


Fig. A.1. Evolution of the permeability K normalized by the pore size squared d^2 as a function of the foam density V_s , according to Eq. (9). Comparison of evaluating the window surface area, a using Arzt’s rigorous derivation [46] or Ashby’s simplified expression [47].

a , of windows between two pores, i.e., of bottleneck limiting the rate of viscous fluid flow through the foam:

$$K = \frac{(a/\pi)^{3/2} \Delta}{\pi r}, \tag{A.1}$$

keeping the same notation as above. Eq. (9) is a special case of Eq. (A.1), derived using Ashby’s expression [47] for evaluating the window surface area, a . Ashby’s equations are a simplification of Arzt’s rigorously derived but more complex equations [46]. In particular, Arzt distinguishes between two modes of material redistribution during powder densification, namely long-range and short-range redistribution. In the present case, the long range redistribution hypothesis is suitable since pressure densification was used in preparing the NaCl preforms.

Predictions for the foam permeability normalized by the square of the pore size d are compared in Fig. A.1. Clearly, evaluating K via Eq. (A.1) using Ashby’s or Arzt’s equations for the window area a as a function of foam relative density Δ leads to essentially the same result; the simpler expression in Eq. (9) is thus fully adequate.

References

- [1] Lage JL, Weinert AK, Price DC, Weber RM. Int J Heat Mass Transfer 1996;39:3633.
- [2] Antohe BV, Lage JL, Price DC, Weber RM. Int J Heat and Fluid Flow 1996;17:594.
- [3] Antohe BV, Lage JL, Price DC, Weber RM. Trans ASME – J Fluids Eng 1996;119:404.
- [4] Lu TJ, Stone HA, Ashby MF. Acta Mater 1998;46:3619.
- [5] Kim SY, Paek JW, Kang BH. J Heat Transfer 2000;122:572.

- [6] Kim SY, Kang BH, Kim J-H. *Int J Heat Mass Transfer* 2001;44:1451.
- [7] Rachedi R, Chikh S. *Heat Mass Transfer* 2001;37:371.
- [8] Girlich D, Franzke U. *Adv Eng Mater* 2001;3:351.
- [9] Boomsma K, Poulikakos D, Zwick F. *Mech Mater* 2003;35:1161.
- [10] Kumar A, Reddy RG. *J Power Sources* 2003;114:54.
- [11] Ashby MF, Evans A, Fleck NA, Gibson LJ, Hutchinson JW, Wadley HNG. *Metal foams: a design guide*. Boston (USA): Butterworth-Heinemann; 2000.
- [12] Banhart J. Functional applications. In: Degischer HP, Kriszt B, editors. *Handbook of cellular metals, production, processing, applications*. Weinheim (Germany): Wiley-VCH; 2002. p. 313 [chapter 7.2].
- [13] Scheidegger AE. *The physics of flow through porous media*. third ed. Toronto: University of Toronto Press; 1974.
- [14] Bear J. *Dynamics of fluids in porous media*. New York: Dover; 1988.
- [15] Lage JL. The fundamental theory of flow through permeable media from Darcy to turbulence. In: Pop I, editor. *Trans Phen Porous Media*. Oxford: Elsevier; 1995. p. 1.
- [16] Lage JL, Antohe BV, Nield DA. *Trans ASME – J Fluids Eng* 1997;119:700.
- [17] Torquato S. *Random heterogeneous materials – microstructure and macroscopic properties*. New York: Springer; 2002.
- [18] Beavers GS, Wilson TA. *J Appl Mech* 1975;42:598.
- [19] Beavers GS, Hajii A, Sparrow EM. *J Fluids Eng* 1981;103:432.
- [20] Beavers GS, Wittenberg K, Sparrow EM. *J Fluids Eng* 1981;103:440.
- [21] Sommer JL, Mortensen A. *J Fluid Mech* 1996;311:193.
- [22] Beavers GS, Sparrow EM. *J Appl Mech* 1969;36:711.
- [23] Montillet A, Comiti J, Legrand J. *J Mater Sci* 1992;27:4460.
- [24] Fourie JG, Du Plessis JP. *Chem Eng Sci* 2002;57:2781.
- [25] Paek JW, Kang BH, Kim SY, Hyun JM. *Int J Thermophys* 2000;21:453.
- [26] Bhattacharya A, Calmidi VV, Mahajan RL. *Int J Heat Mass Transfer* 2002;45:1017.
- [27] Boomsma K, Poulikakos D. *J Fluids Eng* 2002;124:263.
- [28] Kozeny J. *Sitzungsber Akad Wiss Wien* 1927;136:271.
- [29] Carman PC. *Trans Inst Chem Eng London* 1937;15:150.
- [30] Bird RB, Stewart WE, Lightfoot EN. *Transport phenomena*. New York (NY): Wiley; 1960.
- [31] Du Plessis JP, Masliyah JH. *Trans Porous Media* 1988;3:145.
- [32] Du Plessis JP, Montillet A, Comiti J, Legrand J. *Chem Eng Sci* 1994;49:3545.
- [33] Diedericks GPJ, DuPlessis JP. *Math Eng Ind* 1997;6:133.
- [34] Boomsma K, Poulikakos D, Ventikos Y. *Int J Heat Fluid Flow* 2003;24:825.
- [35] Moreira EA, Innocentini MDM, Coury JR. *J Eur Ceram Soc* 2004;24:3209.
- [36] Sangani AS, Acrivos A. *Int J Multiphase Flow* 1982;8:193.
- [37] Sangani AS, Yao C. *Phys Fluids* 1988;31:2435.
- [38] Keller JB. *J Fluid Mech* 1964;18:94.
- [39] Advani SG, editor. *Flow and rheology in polymer composite manufacturing*. Pipes RB, editors. *Composite materials series*, vol. 10. Delaware: Elsevier; 1994.
- [40] Paserin V, Marcuson S, Shu J, Wilkinson DS. The chemical vapor deposition technique for Inco nickel foam production – manufacturing benefits and potential applications. *Cellular metals: manufacture, properties, applications*, Proc. of the conf. metfoam 2003. Berlin, Germany: Verlag-MIT; 2003.
- [41] Sherman AJ, Tuffias RH, Kaplan R. *Ceram Bull* 1991;70:1025.
- [42] LeMay JD, Hopper RW, Hrubesh LW, Pekala RW. *Mater Res Soc Bull* 1990;15:19.
- [43] SanMarchi C, Mortensen A. Infiltration and the replication process for producing metal sponges. In: Kriszt B, editor. *Handbook of cellular metals*. Weinheim, Germany: Wiley-VCH; 2002. p. 43 [chapter 2.06].
- [44] SanMarchi C, Mortensen A. *Acta Mater* 2001;49:3959. p. 3959.
- [45] Happel J, Brenner H. *Low Reynolds number hydrodynamics with special applications to particulate media*. Leyden: Noordhoff International Publishing; 1973. 2nd revised edition.
- [46] Arzt E. *Acta Metall* 1982;30:1883.
- [47] Ashby MF. Sintering and hot isostatic pressing diagrams. In: Wood JV, editor. *Powder metallurgy: an overview*. 1991. p. 144.
- [48] Darcy H. *Les fontaines publiques de la ville de Dijon*. Paris: Dalmont; 1856.
- [49] Nutting PG. *Bull Am Assoc Petrol Geol* 1930;14:1337.
- [50] Wyckoff RD et al. *Rev Sci Instr* 1933;4:394.
- [51] Lide DR, editor. *Handbook of chemistry and physics*. 73rd ed. Boca Raton (FL): CRC Press; 1992–1993.